Nuclear Instruments and Methods in Physics Research B 269 (2011) 2345–2349

Contents lists available at ScienceDirect

Nuclear Instruments and Methods in Physics Research B

journal homepage: www.elsevier.com/locate/nimb

# A characterisation of electronic properties of alkaline texturized polycrystalline silicon solar cells using IBIC

A.M. Jakob [a], D. Spemann [a,*], R. Thies [a], J. Barzola-Quiquia [b], J. Vogt [a], T. Butz [a]

[a] Universität Leipzig, Institute for Experimental Physics II, Division of Nuclear Solid State Physics, Linnéstr. 5, 04103 Leipzig, Germany
[b] Universität Leipzig, Institute for Experimental Physics II, Division of Superconductivity and Magnetism, Linnéstr. 5, 04103 Leipzig, Germany

ARTICLE INFO

*Article history:*
Available online 28 February 2011

*Keywords:*
IBIC
Polycrystalline silicon solar cells
Capture cross section
Diffusion length

ABSTRACT

In this study, electronic properties of p-type alkaline texturized polycrystalline silicon solar cells were investigated using ion beam induced charge (IBIC) analysis. With this technique, quantitative information on electronic diffusion lengths and average electronic capture cross sections of lattice defects generated by high energy protons were obtained. Angular-resolved IBIC analysis was used to quantify the electronic diffusion lengths. For this purpose, the experimental data were fitted using a simulation based on the Ramo–Shockley–Gunn (RSG) theorem and the assumption of an abrupt pn-junction. In order to determine the average electronic capture cross section of proton-induced lattice defects, the loss of charge collection efficiency (CCE) was plotted vs. the accumulated ion fluence. As will be demonstrated, a simple model based on charge carrier diffusion and Shockley–Read–Hall (SRH) recombination is able to fit the CCE loss well. Furthermore, spatially and energetically highly resolved IBIC-maps of grain boundaries were recorded. A comparison with PIXE-maps shows that there is no correlation observable between CCE variations at grain boundaries and metallic impurities within the PIXE detection limits of a few ppm. On the contrary, there is an evident correlation to the morphology of the sample's surface as was observed by comparing IBIC-maps and SEM-micrographs. These local CCE fluctuations are dominated by the interplay of charge carrier diffusion processes and the sample surface morphology.



## 1. Introduction

Previous EBIC (Electron Beam Induced Current) measurements carried out on these polycrystalline silicon solar cells done by the manufacturer indicated that charge collection on grain boundaries differs from that within grains. In some cases, increased charge collection efficiency (CCE) is observed. However, most boundaries show reduced CCE. The assumption was that these results are caused by an enrichment of metallic impurities between adjacent grains. Due to the poor signal-to-noise ratio (SNR) of the solar cell samples and small energy of the irradiating electrons, more detailed maps could not be recorded using EBIC.

Highly energetic ions are a powerful tool regarding elemental and structural investigation of materials. The IBIC technique permits the characterisation of electronic properties of almost arbitrary semiconductor devices based on pn-junctions and Schottky-contacts, respectively. The LIPSION nanoprobe [1] allows IBIC measurements with spatial resolutions down to 150 nm for appropriate samples. Hence, combined PIXE-, IBIC-, and SEM analysis are an ideal instrument for getting a deeper understanding of local CCE variations of polycrystalline silicon solar cells.

## 2. Theory

### 2.1. Ion beam induced charge (IBIC)

In order to gain quantitative information from experimental IBIC data a correlation between the ion beam induced free charge carrier concentration within the semiconductor volume and the amount of collected charge at the electrodes must be established. This relationship can be described by the general Ramo–Shockley–Gunn theorem for arbitrary charge distributions and electrode geometries [2–4]. More detailed information on this can be found in [5,6]. The CCE $\eta$ is defined by the ratio of the induced charge $Q_{ind}$ and the charge generated by ionization $Q_{gen}$. In the following let us consider an abrupt planar pn-junction as shown in Fig. 1. A CCE contribution of charge carriers generated in the highly n-doped region ($n^{++}$) is assumed to be negligible due to the small layer thickness and high recombination rates. Moreover, no interactions between generated free carriers are taken into account. A static external bias source generates a electric field, so that carrier transport within the depletion region of width $w$ is dominated by drift.

* Corresponding author. Tel.: +49 341 97 32706; fax: +49 341 97 32708.
*E-mail address:* spemann@uni-leipzig.de (D. Spemann).

0168-583X/$ - see front matter © 2011 Elsevier B.V. All rights reserved.
doi:10.1016/j.nimb.2011.02.040

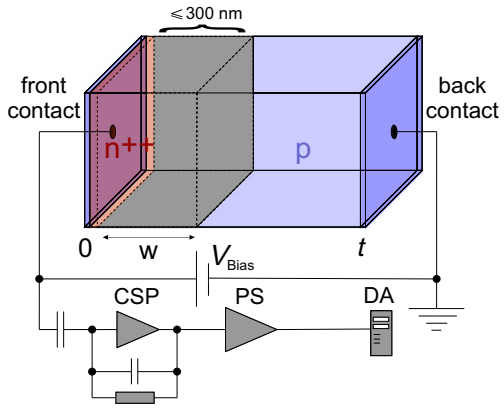


**Fig. 1.** Schematic of the IBIC measuring setup and a sample with an abrupt pn-junction. 'CSP' – Charge Sensitive Preamplifier, 'PS' – Pulse Shaper, 'DA' – Data Acquisition.

Since the drift time is much shorter than the carrier lifetime, the carrier recombination in the depletion region is negligible. Furthermore, it is supposed that the sample thickness $t$ exceeds the maximum ion range $R$. Thus, the CCE $\eta$ is described by Vittone et al. [6], Breese et al. [7]:

$$\eta = \frac{1}{E_0}\left[\int_0^{\frac{w}{\cos\alpha}} \frac{dE}{dx}dx + \int_{\frac{w}{\cos\alpha}}^{R} \frac{dE}{dx} e^{-\frac{x\cos\alpha - w}{L_n(x)}}dx\right] \quad (1)$$

whereas $\alpha$ denotes the angle between sample surface normal and ion beam axis and $L_n(x)$ is the diffusion length of electrons. $E_0$ is the initial energy of impinging ions after passing a dead layer $d$ along the trajectory $s = \frac{d}{\cos\alpha}$. The energy loss $\frac{dE}{dx}$ of highly energetic ions in the target materials can be evaluated numerically using the SRIM2010 software [8].

### 2.2. Charge carrier recombination

A quantitative characterisation of carrier recombination processes on lattice defects can be realised by the Shockley–Read–Hall (SRH) theory [9,10]. Here, local and temporal variations of free carrier concentrations are described by continuity equations which take into account carrier generation and recombination processes as well as carrier transport phenomena. A free charge carrier lifetime $\tau$ can be defined depending on defect state concentrations $N_{T,i}$, their effective charge carrier capture cross sections $\sigma_{T,i}$ as well as the thermal velocity $v_{th,n}$ of charge carriers. In addition to various defect types $i$ initially present in the sample there are defect states $j$ induced by ion irradiation as well. With $N_{Ion,j}$ and $\sigma_{Ion,j}$ being their concentrations and capture cross sections, respectively, the lifetime $\tau$ is given by:

$$\tau = \frac{1}{\left[\sum_i N_{T,i}\sigma_{T,i} + \sum_j N_{Ion,j}\sigma_{Ion,j}\right] v_{th,n}} \quad (2)$$

## 3. Experimental

### 3.1. Examined samples

The samples investigated here are commercial polycrystalline silicon solar cells whose surfaces were texturized with alkaline etching. A $Si_3N_4$ top layer of less than 100 nm thickness is deposited on the front surface and protects the substrate against external mechanical stresses. Furthermore, surface recombination processes are minimised. The 200 μm thick bulk substrates consist of p-type silicon with an uniform acceptor concentration of $N_{acc} \approx 10^{16}$ cm$^{-3}$ as has been confirmed from capacitance-voltage data obtained from admittance spectroscopy. The implantation of phosphorous at the front surface leads to a formation of a highly n-doped region. SNMS (Secondary Neutral Mass Spectrometry) measurements show an exponential decrease of the phosphorous detection rate with increasing sputtering depth. The maximum rate of 100 counts s$^{-1}$ reduces down to 10% within 50 nm. Hence a non-linear electric field distribution inside the pn-depletion layer is expected. Nevertheless, it can be assumed that the pn-junction is abrupt and its capacitance is alike a planar capacitor [11]. This assumption is supported by the measured capacitance-voltage data. The average depletion layer width can thus be estimated to be less than 300 nm. Consequently, high capacitances of about 40 nF cm$^{-2}$ are typical values for these samples and lead to poor SNR as mentioned earlier. In order to keep IBIC measurements feasible, small samples of about 2 × 2 mm$^2$ size and thus lower capacitances were examined.

The electric back contact is realized by baking a thin aluminum plate on the rear surface of the bulk. The baking process leads to a diffusion of Al into the silicon substrate and generates a highly p-doped layer. Between this region and the p-doped bulk substrate, a back surface field (BSF), similar to the electric field within the pn-junction, forms. Previous IBIC measurements indicate that the BSF does not influence the quantitative analysis presented here. It should be noted that the BSF has no impact on the admittance measurements as well due to the sample thickness.

The samples investigated were pre-selected using admittance spectroscopy and the I-U-characteristic. The main selection criteria were a low leakage current and no grain boundaries within the sample for studies of the electronic properties. The samples selected showed a similar electronic behaviour.

In the following, it is assumed that carriers which reach the depletion layer region are collected completely and that the layout of these samples follows the schematic shown in Fig. 1.

### 3.2. Measuring setup

The IBIC measurements were carried out at the LIPSION nanoprobe laboratory. The amplification of IBIC signals was realized using an AMPTEK A250 charge sensitive preamplifier and a modified electronic setup based on the circuit diagram described in [12]. To keep wiring capacitances as low as possible the whole assembly is mounted on a small circuit board, where a bistable micro-relais allows a remote-controlled switching between sample and reference detector. Commercially available HAMAMATSU S1223-01 pin diodes are used as reference detectors for CCE calibration of the examined samples. The CCE of the pin diodes is assumed to be $\eta = 1$. They can be plugged on a socket located at the board. The sample's back electrode contact is realised by a gold coated base plate next to the detector socket. Front contacts are established using 25 μm thick gold wires and silver conductive paint. The electronic board is embedded in a metal box and shielded against electromagnetic radiation. The preamplified signal is fed into an external EG&G Ortec 572 Shaper and digitised by a Canberra 8701 ADC.

SEM micrographs were taken with the SEM/FIB Dual Beam Microscope Nanolab 200.

## 4. Results and discussion

### 4.1. Minority carrier diffusion length

In order to determine minority carrier diffusion lengths, angular resolved IBIC measurements were carried out using 2250 keV protons. For this purpose, the IBIC spectra were recorded at different

tilt angles $\alpha$ between beam axis and sample normal in the range of $0^\circ \leqslant \alpha \leqslant 80^\circ$. To ensure a negligible influence of proton induced lattice defects on the CCE the ion beam was scanned over the whole sample area. Hence the fluence was kept below 1 ion $\mu m^{-2}$. The measured CCE and thus the calculated diffusion lengths are, therefore, average values for each sample.

Eq. (1) was used to simulate the measured CCE versus tilt angle as plotted in Fig. 2. The $Si_3N_4$ dead layer thickness $d$ was determined using RBS measurements to be 70 nm. Since the range of 2250 keV protons is much higher than the depletion layer width $w$ or the dead layer thickness $d$, variations within limits of $100\ nm \leqslant w \leqslant 300\ nm$ and $50\ nm \leqslant d \leqslant 150\ nm$ do not affect the simulated curves significantly, even at higher tilt angles.

Therefore, the primary simulation parameter is the minority carrier diffusion length which was obtained to be $L_n = 45 \pm 5\ \mu m$ for virgin samples. These results agree well with values from other commercially available polycrystalline silicon solar cells reported in [13].

### 4.2. Electronic properties of lattice defects

In order to study the trapping behaviour of lattice defects induced by high-energy protons on the minority carriers the CCE loss versus accumulated ion fluence $\Phi$ was acquired using 2250 keV protons. Here, the irradiated area was located within a large grain and amounts only to $200 \times 200\ \mu m^2$ which minimizes influences from grain boundaries and keeps acquisition times within feasible limits. Fig. 3 displays the experimental data and the simulated curve. In order to extract quantitative information from the experimental data a correlation between RSG-theorem and SRH-theory is required. Since the proton range is much larger than the depletion layer thickness, diffusion processes dominate the carrier transport and the first integral of Eq. (1) can be neglected at 0° tilt angle. The accumulated ion fluence leads to a further reduction of the minority carrier diffusion length $L_n$, whereas the characteristic defect generation profile $N_{DP}$ of one ion multiplied by the ion fluence $\phi$ causes an additional depth dependence of $L_n$. Using Eq. (2) of the SRH-theory, the electron diffusion constant $D_n$, the electron carrier lifetime $\tau_n$, and

$$L_n = \sqrt{D_n \tau_n} \tag{3}$$

the diffusion length is calculated to:

$$L_n(x) = \sqrt{\frac{D_n}{[\sigma_T N_T + \sigma_{Ion} N_{Ion}(x)]\, v_{th,n}}} \tag{4}$$

where the proton induced defect concentration $N_{Ion}(x)$ depends on the defect generation profile as follows:

$$N_{Ion}(x) = \phi N_{DP}(x) \tag{5}$$

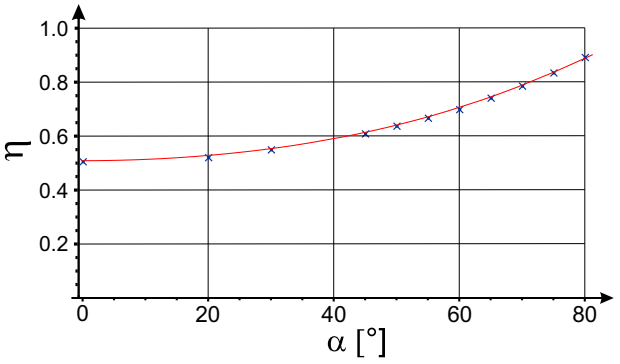


**Fig. 2.** Measured CCE as a function of the tilt angle $\alpha$ together with a fit according to Eq. (1).

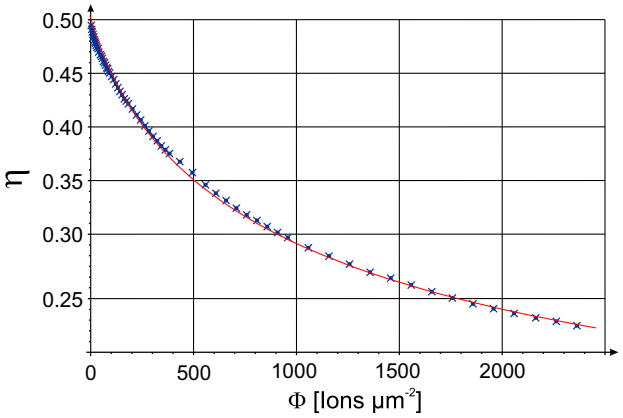


**Fig. 3.** Experimental data of CCE loss vs. accumulated ion fluence and fit curve for the determination of carrier capture cross sections.

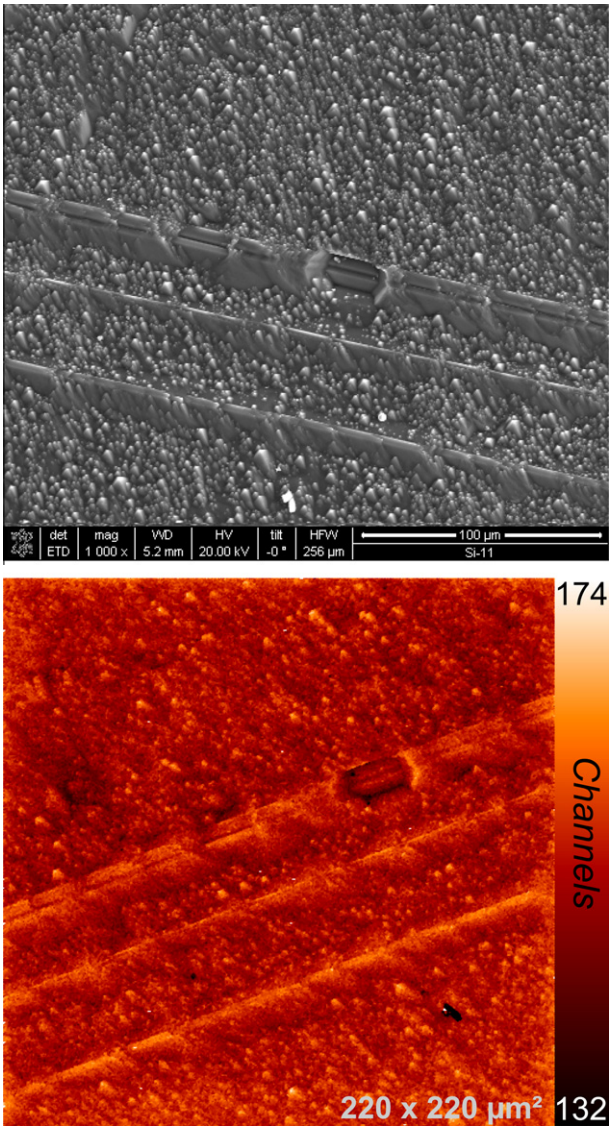


**Fig. 4.** Top: SEM micrograph of multiple grain boundaries. Bottom: IBIC map of the same region.

$N_{DP}$ can be obtained numerically using the SRIM2010 code [8]. Putting Eqs. (5) and (4) in (1) the CCE loss versus ion fluence can be

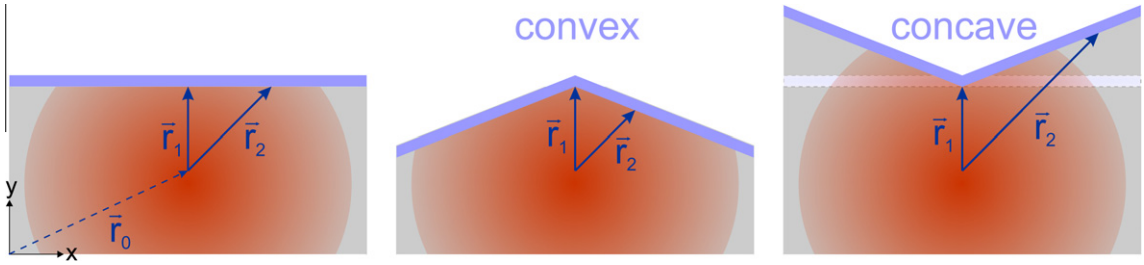


**Fig. 5.** Schematic illustration of local CCE variations due to surface topology in case of a dominating charge carrier diffusion.

simulated. The electronic thermal velocity $v_{th,n}$ amounts to $2.3 \times 10^7$ cm s$^{-1}$ in silicon [14] and the electronic diffusion constant in p-type silicon is approximately $D_n \approx 30$ cm$^2$ s$^{-1}$ [15]. The initial defect concentration $N_T$ is assumed to be dominated by the boron dopands, since no detailed information about the initial defect concentration of the samples was available. Free fitting parameters are the minority carrier capture cross sections $\sigma_T$ and $\sigma_{Ion}$. They were obtained to be $\sigma_T = (5.6 \pm 0.9) \times 10^{-18}$ cm$^2$ and $\sigma_{Ion} = (3.0 \pm 0.5) \times 10^{-16}$ cm$^2$ by fitting the simulated curve to the experimental data as shown in Fig. 3. In principle, the carrier lifetime $\tau_n$ of undamaged material can be used to determine $\sigma_T N_T$ following Eqs. (2) and (3). This approach would reduce the number of free parameters in the fit. However, the diffusion length could only be determined after substantial ion beam induced damage in this sample and could therefore not be taken as a measure for $\sigma_T N_T$.

The observed value for proton induced defects exceeds the one of initial defects by a factor of 50. This can be easily understood, because ion induced lattice dislocations influence local band characteristics and hence minority carrier recombination rates much more than substitutionally localized boron atoms. However, it is not clear whether these values are quantitatively correct or not as this method is not able to differentiate between various types of defects. Measured minority capture cross sections of proton induced defects are thus only average values. Moreover, the concentrations and characteristic capture cross sections of the initial defects must be known. These values can be obtained using minority carrier transient spectroscopy (MCTS) measurements for example. Combined IBIC and MCTS measurements on well defined reference samples are necessary to inspect the analysis presented here in more detail.

### 4.3. Influence of topology on local CCE

Spatially resolved IBIC maps were recorded using 1800 keV He$^+$ ions. As already mentioned, PIXE maps from various of these samples did not show any significant impurity concentrations within the detection limits of PIXE. Based on these results, comparisons of IBIC-maps and SEM-micrographs at grain boundaries were done. It should be noted that the peak-to-peak roughness of these samples was up to 20 μm at grain boundaries and thus much higher than expected. These surface properties are a result of the alkaline etching process where the etching rate strongly depends on the local crystal orientation. A correlation between CCE maps and the surface topology was observed as can be seen in Fig. 4. Elevated regions visible in the SEM image show increased collection efficiency. Further comparisons of IBIC maps and SEM micrographs on various samples lead to the conclusion that convex structures always show a higher CCE whereas concave topologies are regions of reduced charge collection.

This effect can be understood when taking into account the different topological morphologies and the dominance of charge diffusion processes. Let us consider a delta-like generation point of free charge carriers at a point $\vec{r}_0$ as shown in Fig. 5. Along trajectory $\vec{r}_1$ more charge carriers will arrive at the pn-junction than along $\vec{r}_2$ due to the smaller distance. Convex surfaces bend toward the generation centre (Fig. 5) which reduces the distance to the pn-junction for charges travelling in $\vec{r}_2$ direction. This leads to enhanced CCE at convex surfaces. Concave structures show exactly the opposite behaviour. The distance along $\vec{r}_2$ is increased which leads to a reduction of the collected charge at the pn-junction. In addition, inhomogeneities of the electric field in the pn-junction due to the topology will in principle influence the CCE as well. However, this effect should be negligible here, because of the long diffusion distances and the small depletion layer width. It is worth mentioning that the lateral ion straggling is about 550 nm for 1800 keV He$^+$ ions and the beam diameter amounts to approximately 150 nm. For lateral dimensions of surface features exceeding a value of about 700 nm, their resolvability is mainly limited by carrier diffusion under these experimental conditions. In this case local surface roughnesses determine the contrast of topological details in IBIC maps. The influence of topological characteristics on local CCE dominates the one of lattice defects on grain boundaries. Hence, no local CCE dependence on these defect states was observable in the samples investigated here.

## 5. Conclusions

We demonstrated that a modelling of IBIC data allows one to determine electronic properties like carrier diffusion lengths $L_n$ and carrier capture cross sections $\sigma$ on commercially available polycrystalline silicon solar cells. Furthermore, it could be shown that local CCE fluctuations of alkaline texturized silicon solar cells are dominated by sample topologies and charge diffusion processes. No increased metallic impurity concentrations were found at grain boundaries within detection limits of the PIXE technique. The influence of recombination processes at grain boundaries on the CCE due to a higher concentration of recombination centres is negligible in comparison to the influence of topological features.

## Acknowledgement

The help and support of Florian Schmidt and Holger von Wenckstern in the admittance spectroscopy measurements is gratefully acknowledged.

## References

[1] D. Spemann, T. Reinert, J. Vogt, T. Andrea, N. Barapatre, R. Feder, A.M. Jakob, N. Liebing, Ch. Meinecke, F. Menzel, M. Rothermel, T. Butz, Nucl. Instr. Meth. B, this proceedings. doi:10.1016/j.nimb.2011.02.054.
[2] W. Shockley, J. Appl. Phys. 9 (1938) 635.
[3] S. Ramo, Proc. IRE 27 (1939) 584.
[4] J.B. Gunn, Solid State Electron. 7 (1964) 739.
[5] G. Cavalleri, E. Gatti, G. Fabri, V. Svelto, Nucl. Instr. Meth. B 92 (1971) 137.
[6] E. Vittone, F. Fizzotti, A. Lo Giudice, C. Paolini, C. Manfredotti, Nucl. Instr. and Meth. B 161–163 (2000) 446.
[7] M.B.H. Breese, E. Vittone, G. Vizkelethy, P.J. Sellin, Nucl. Instr. and Meth. B 264 (2007) 345.

[8] J.F. Ziegler. Available from: <http://www.srim.org/>.
[9] W. Shockley, W.T. Read Jr., Phys. Rev. 87 (1952) 835.
[10] R.N. Hall, Phys. Rev. 87 (1952) 387.
[11] E. Vittone, Nucl. Instr. Meth. B 219–220 (2004) 1043.
[12] AMPTEK Inc. 14 DeAngelo Drive, Bedford, MA 01730-2204, USA. Available from: <http://www.amptek.com/pdf/pc250.pdf>.
[13] K.K. Lee, D.N. Jamieson, Nucl. Instr. Meth. B 158 (1999) 445.
[14] Ioffe Physical Technical Institut, Tech. rep. Available from: <http://www.ioffe.ru/SVA/NSM/Semicond/Si/electric.html>.
[15] J. Mohrhof, Experimentelle Untersuchungen zu Minoritätsträger-Diffusionskonstanten in Silizium, Ph.D. Thesis, Universität Bremen, 2004.